Visualizing Recurrently Migrating Hydrogen in Acetylene Dication by Intense Ultrashort Laser Pulses

Akiyoshi Hishikawa,[1,2,3,*] Akitaka Matsuda,[1] Mizuho Fushitani,[1,2] and Eiji J. Takahashi[1,2]

[1]*Institute for Molecular Science, National Institutes of Natural Sciences, Myodaiji, Okazaki, Aichi 444-8585, Japan*
[2]*The Graduate University for Advanced Studies (SOKENDAI), Myodaiji, Okazaki, Aichi 444-8585, Japan*
[3]*PRESTO, Japan Science and Technology Agency, Kawaguchi, Saitama 332-0012, Japan*

(Received 23 January 2007; published 21 December 2007)

We demonstrate the visualization of ultrafast hydrogen migration in deuterated acetylene dication ($C_2D_2^{2+}$) by employing the pump-probe Coulomb explosion imaging with sub-10-fs intense laser pulses (9 fs, 0.13 PW/cm^2, 800 nm). It is shown, from the temporal evolution of the momenta of the fragment ions produced by the three-body explosion, $C_2D_2^{3+} \rightarrow D^+ + C^+ + CD^+$, that the migration proceeds in a recurrent manner: The deuterium atom first shifts from one carbon site to the other in a short time scale (~90 fs) and then migrates back to the original carbon site by 280 fs, in competition with the molecular dissociation.

DOI: 10.1103/PhysRevLett.99.258302 PACS numbers: 82.53.−k, 33.80.Rv, 42.50.Hz, 82.50.Pt

Hydrogen migration [1] is a molecular rearrangement process that occurs in a variety of chemical reactions, for example, in combustion [2] and catalytic [3] processes as well as in strong laser fields [4,5]. Because of the large mobility of hydrogen, the migration often proceeds in a very short time scale to determine the main routes of intra- and intermolecular reactions by suppressing other competing processes [1]. Despite the importance in the understanding of chemical reactions, however, migrating hydrogen atoms have eluded visualization, even after the advent of the ultrafast electron and x-ray diffraction techniques, because of the ultrafast time scale in the subpicosecond range [4,6,7] and the low x-ray/electron scattering efficiency.

Recent advances in laser technology have enabled us to utilize ultrashort intense laser pulses (<10 fs, ~10^{15} W/cm^2) as a new probe to image the ultrafast structural deformation in reaction processes. Molecules exposed to such intense laser pulses promptly eject several electrons by nonresonant interactions and undergo rapid bond breaking (called Coulomb explosion) on the repulsive Coulombic potential energy surface of the highly charged states [8]. Since the momenta of the resultant fragment ions reflect sensitively the geometrical structure of the target molecule [9,10], the Coulomb explosion provides direct access to the instantaneous structure in the course of reaction processes, as demonstrated for dissociating diatomic [11,12] and triatomic molecules [13,14].

The isomerization of neutral acetylene [1,6,15,16] and its ionic species [7,17–20] between the acetylene (HCCH) and vinylidene (H_2CC) configurations has been extensively studied as a prototype of the hydrogen migration proceeding via the shift of a hydrogen atom from one carbon site to the other, while reports of direct time-scale measurements are sparse [16,18]. In the present Letter, we demonstrate the real-time visualization of ultrafast hydrogen migration in acetylene dication by employing the pump-probe Coulomb explosion imaging [13,14]. In order to track the ultrafast dynamics (estimated to proceed within 60 fs [7]), we use the deuterated acetylene (C_2D_2) as the target and employed extremely short intense laser pulses in the sub-10 fs regime.

Our experimental scheme is shown in Fig. 1(a). A pair of ultrashort intense laser pulses (9 fs, 0.13 PW/cm^2, 800 nm) are employed as the pump and probe pulses. The pump laser pulse is used to doubly ionize the target molecule as well as to trigger the hydrogen migration. The structural change of $C_2D_2^{2+}$ is then probed by another intense laser pulse, introduced with a time delay Δt to ionize $C_2D_2^{2+}$ to $C_2D_2^{3+}$. The three-body Coulomb explosion process from $C_2D_2^{3+}$, $C_2D_2^{3+} \rightarrow D^+ + C^+ + CD^+$, is monitored for each explosion event by the coincidence momentum imaging method [21] to identify the location of the deuterium atom migrating between the two carbon sites, $DCCD^{2+} \leftrightarrow D_2CC^{2+}$.

Here we focus our attention to the angle θ_{12} between the momenta of the resultant D^+ and C^+ fragment ions, $\boldsymbol{p}_1(D^+)$ and $\boldsymbol{p}_2(C^+)$. For the acetylene configuration, the angle θ_{12} is expected to be small due to its linear geometry, whereas large θ_{12} values should be observed when the hydrogen migration proceeds towards the vinylidene configuration [see Fig. 1(b)]. In order to see how the location of the migrating deuterium is mapped to the momentum angle θ_{12}, we simulated the three-body Coulomb explosion by numerically solving the classical equation of motion, in which each fragment ion is treated as a point charge. The results obtained at different positions (r, α) of D in the molecular frame are shown in Fig. 1(b). The acetylene ($\alpha = 0°$) and vinylidene ($\alpha \sim 140°$) configurations [20] lead to the Coulomb explosion with different momentum angles, $\theta_{12} = 0°$ and 130°, respectively. These values are insensitive to the radial coordinate r, showing that a slight increase in the C-D bond length that may occur in the sub-10-fs probing process [9] causes little effect on the θ_{12} distribution.

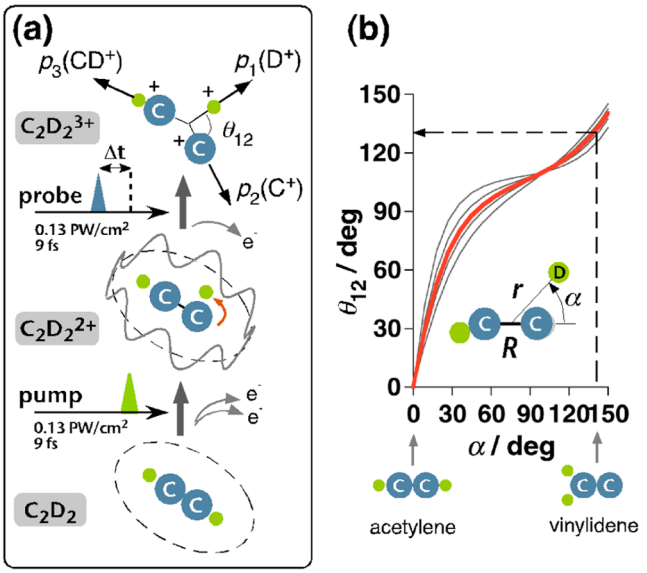

FIG. 1 (color online). (a) Pump-probe Coulomb explosion imaging employed in the present study. The pump pulse creates $C_2D_2^{2+}$ and triggers the hydrogen migration. The instantaneous location of migrating deuterium atoms is determined from the momenta of fragment ions, D^+, C^+, CD^+, ejected in the Coulomb explosion of $C_2D_2^{3+}$ induced by the probe pulse. (b) Momentum angle θ_{12} as a function of the polar angle α obtained by the classical simulation of three-body Coulomb explosion (red line) for the structural parameters, $r = 1.8$ Å and $R = 1.34$ Å, that correspond to the geometry of acetylene dication in the ground $X^3\Sigma_g^-$ state [20]. Results obtained for other radial distances (gray lines), $r = 1.4$, 1.6, 2.0, and 2.5 Å (from top to bottom), show that the vinylidene configuration ($\alpha \sim 140°$) corresponds to the momentum angle of $\theta_{12} \sim 130°$, irrespective of the radial distance.

The experimental setup described previously [22] was used with modifications for the ultrafast pump-probe measurements. The output from an ultrashort Ti:sapphire femtosecond laser system (~10 fs, 800 nm, 1 kHz, 0.4 mJ/pulse) [22] was introduced to a high-precision Michelson-type interferometer to generate the linearly polarized pump and probe laser pulses, which were then focused onto an effusive molecular beam of C_2D_2 in an ultrahigh vacuum chamber ($<10^{-8}$ Pa). The dispersion induced by the optical materials was precompensated to obtain the intense ultrashort pulses (9 fs, 0.13 PW/cm^2) at the focus. The minimum time delay between the pump and probe pulses, $\Delta t = 30$ fs, was chosen to avoid strong optical interferences between the pump and probe pulses [11]. The residual effects (<7%) of the pulse overlap at short time delays $\Delta t < 60$ fs were removed by the data averaging at two different time delays $\Delta t \pm T/4$ (corresponding to constructive and destructive interferences) at each Δt, where T is the laser optical period (~2.7 fs). The fragment ions produced from the target molecule were guided by four electrodes in velocity mapping configuration to a fast position sensitive detector, where all the fragment ions originating from a single parent ion were detected in coincidence. The momenta, $\boldsymbol{p}_1(D^+)$, $\boldsymbol{p}_2(C^+)$, and $\boldsymbol{p}_3(CD^+)$, were determined as three-dimensional vectors for each Coulomb explosion event from the (x, y) position and the time of flight t at the arrival of the respective fragment ions at the detector. The momentum conservation condition, $|\Sigma \boldsymbol{p}_i| < 5$ a.u., was used to discriminate true coincidence events from false events. The momentum angle θ_{12} and the total kinetic energy release E_{kin} were calculated from the measured momenta as $\theta_{12} = \cos^{-1}[\boldsymbol{p}_1(D^+) \cdot \boldsymbol{p}_2(C^+)/(p_1 p_2)]$ and $E_{\mathrm{kin}} = \Sigma {p_i}^2/(2m_i)$, where m_i and p_i are the mass and the absolute value of the momentum for the ith fragment ion, respectively.

Figure 2(a) depicts the changes in the observed θ_{12} distributions as a function of the pump-probe delay Δt. Since the available phase space sharply decreases as $\sin\theta_{12}$ [10], the θ_{12} distribution always peaks at a finite value. As Δt increases, a shoulderlike feature emerges near $\theta_{12} = 120°$, as expected for the isomerization from acetylene to vinylidene discussed above and extends further to larger θ_{12} values. A complementary behavior was observed for the momentum angle between $\boldsymbol{p}_1(D^+)$ and $\boldsymbol{p}_3(CD^+)$. For further discussion, however, we need to take into account the dissociation of $C_2D_2^{2+}$, which is known to occur in a short time scale [7,19] for the highly excited states. Indeed, in Fig. 2(b), the distribution of the kinetic energy release E_{kin} shows the appearance of a new component at $\Delta t = 60$ fs on the lower energy side of the original peak ($E_{\mathrm{kin}} \sim 18$ eV), which shifts to $E_{\mathrm{kin}} \sim 8$ eV as Δt increases. The observed decrease in E_{kin} is attributed to the dissociation induced by the pump laser pulse, since the Coulomb repulsion among the fragments is reduced by the increase in the internuclear distances. From the analysis of the mo-

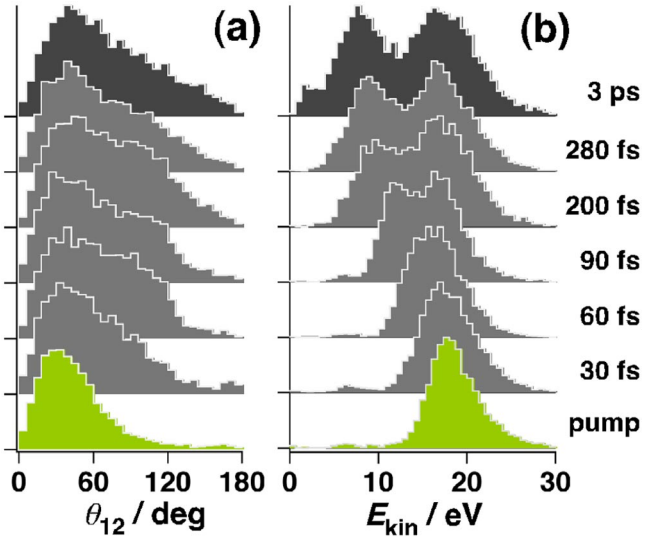

FIG. 2 (color online). Evolution of (a) momentum angle θ_{12} and (b) total kinetic energy release E_{kin} distributions, obtained with ~10^7 laser shots for each pump and probe delay Δt. Each distribution is normalized to the peak value.

mentum distribution in the $p_1(D^+)$-$p_2(C^+)$ correlation map performed along the lines described previously [13], we found that the low energy component originates dominantly (>90%) from $C_2D_2^{2+}$, dissociating through the two-body pathways [19], $C_2D_2^{2+} \rightarrow$ (i) $D^+ + C_2D^+$, (ii) $CD^+ + CD^+$, and (iii) $C^+ + CD_2^+$. This shows that the dynamics in $C_2D_2^{2+}$ is most sensitively detected in the present experimental scheme, with negligibly small contributions from those in lower charged species ($C_2D_2^+$, C_2D_2). The branching ratios of these two-body pathways, 5:2:1, are found in good agreement with the results obtained at ~7 eV above the single photon excitation threshold [19], indicating the contribution from the electronically excited states of $C_2D_2^{2+}$ discussed below.

In order to clarify how the isomerization from the acetylene to vinylidene configuration proceeds in undissociated $C_2D_2^{2+}$, the corresponding coincidence events need to be separated from those of the dissociating component. The difference between the two components is clearly seen in the two-dimensional E_{kin}-θ_{12} map shown in Fig. 3(a); a broad image extending from $\theta_{12} = 0°$ to 180° is observed for $E_{kin} \sim 8$ eV, whereas a dense distribution is identified at small θ_{12} values for $E_{kin} \sim 18$ eV. Accordingly, the coincidence events with $E_{kin} < 13$ eV, corresponding to the dissociating component, form a broad θ_{12} distribution $P_{dis}(\theta_{12})$ in Fig. 3(c) attributable to the rotation of the fragment ions (e.g., C_2D^+) in the two-body dissociation process. On the other hand, a clear peak at a small value $\theta_{12} = 40°$ is identified in $P_{uds}(\theta_{12})$ for the undissociated component (defined with $E_{kin} \geq 13$ eV) as shown in Fig. 3(b).

It is noted that the pump laser pulse alone can induce the three-body Coulomb explosion process monitored in the present study. Consequently, the corresponding θ_{12} distribution, $P_{pump}(\theta_{12})$, shown in Fig. 2(a) (bottom trace), contributes to $P_{uds}(\theta_{12})$ as a background. For the probe laser pulse, we approximated the background contribution as $P_{probe}(\theta_{12}) \sim 0.5 P_{pump}(\theta_{12})$, because about 50% [estimated by integrating the Ammosov-Delone-Krainov (ADK) tunneling ionization rates [23]] of acetylene remains in the neutral state after the interaction with the pump laser pulse. The background-free θ_{12} distribution is therefore given as $P^0_{uds}(\theta_{12}) = P_{uds}(\theta_{12}) - P_{bg}(\theta_{12})$, where $P_{bg}(\theta_{12}) = P_{pump}(\theta_{12}) + P_{probe}(\theta_{12}) \sim 1.5 P_{pump}(\theta_{12})$ [see Fig. 3(b)]. The population of the undissociated component shows that 60% of $C_2D_2^{2+}$ produced by the pump pulse undergoes a rapid dissociative decay with a lifetime of 38(10) fs, while the rest (40%) remains undissociated within the time range investigated.

The evolution of $P^0_{uds}(\theta_{12})$ is depicted in Fig. 4. At the shortest time delay $\Delta t = 30$ fs, $P^0_{uds}(\theta_{12})$ exhibits a peak at small values around $\theta_{12} = 30°$, as observed with the pump laser pulse only. Then, the distribution shifts to large θ_{12} values as Δt increases until $\Delta t \sim 90$ fs when the distribution is peaked at $\theta_{12} \sim 120°$ with a steep edge on the larger angle side. At a larger time delay, the θ_{12} distribution gradually shifts in the reverse direction towards the acetylene configuration to eventually form the distribution peak

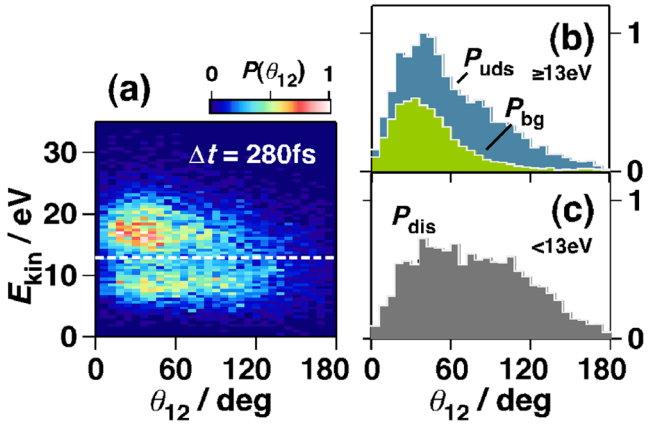

FIG. 3 (color online). (a) All the triple coincidence events (~11 000 events) obtained at $\Delta t = 280$ fs plotted in the E_{kin}-θ_{12} plane. The projections to the horizontal and vertical axes correspond to the θ_{12} and E_{kin} distributions at $\Delta t = 280$ fs in Fig. 2, respectively. The broken line at $E_{kin} = 13$ eV defines the boundary between the undissociated (≥13 eV) and dissociating components (<13 eV). (b) The θ_{12} distribution, $P_{uds}(\theta_{12})$, of the undissociated $C_2D_2^{2+}$ (blue), plotted together with the background contribution, $P_{bg}(\theta_{12})$, from the pump and the probe pulses (green). (c) The θ_{12} distribution $P_{dis}(\theta_{12})$ of the dissociating component. The background contribution is negligibly small in this energy range (see Fig. 2).

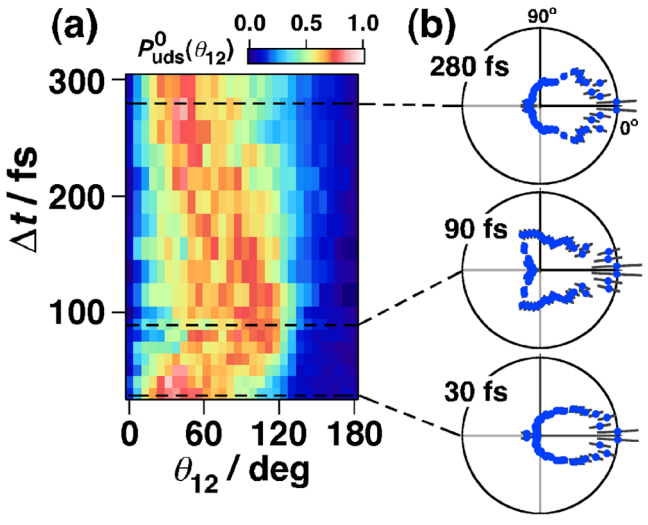

FIG. 4 (color online). (a) Evolution of $P^0_{uds}(\theta_{12})$ normalized by the population recorded in steps of 10 fs for $\Delta t \leq 100$ fs and 20 fs for $\Delta t > 100$ fs, showing that the deuterium atom rapidly migrates from one carbon site to the other within 90 fs and then migrates back to the acetylene configuration in 280 fs. (b) The $P^0_{uds}(\theta_{12})/\sin\theta_{12}$ distributions at three selected time delays, $\Delta t = 30$, 90, and 280 fs, expressed in the polar plot.

again at $\theta_{12} \sim 30°$ at $\Delta t \sim 280$ fs, but with a broader distribution extending to $\theta_{12} \sim 120°$.

In order to discuss the evolution of the deuterium atom distribution in the molecular frame, the observed $P^0_{\mathrm{uds}}(\theta_{12})$ distributions are divided by the phase-space factor $\sin\theta_{12}$ mentioned above. As shown in Fig. 4(b), the deuterium distribution at $\Delta t = 30$ fs forms a peak at $\theta_{12} = 0°$, illustrating that the deuterium atom is located near the original carbon site at the short time delay. On the other hand, an additional peak at $\theta_{12} \sim 120°$ is observed at $\Delta t = 90$ fs, showing that part of the acetylene dication undergoes rapid hydrogen migration to reach the vinylidene configuration in sub-100-fs time scale. The small differences between the observed θ_{12} value ($\theta_{12} \sim 120°$) and the calculated results ($\theta_{12} \sim 130°$) for the vinylidene configuration should be attributed to deviations from the Coulombic potential used in the simulation. The observed time scale is consistent with the upper limit of the isomerization time of 60 fs suggested for $C_2H_2^{2+}$ by the experimental study on the inner-core ionization of carbon K shell [7], since the migration is expected to become slower in $C_2D_2^{2+}$ because of the increase in the effective mass. After reaching the vinylidene configuration, the deuterium atom is found to undergo backward migration to the acetylene configuration with a longer time scale of 190 fs (=280–90 fs) to form a broader distribution around the C-C skeleton. The structural change associated with the recurrent migration was also confirmed as the modulation of the kinetic energies of the C^+ and CD^+ ions. The fraction of the undissociated $C_2D_2^{2+}$ observed in the vinylidene configuration is estimated to be 43% at $\Delta t = 90$ fs from the distribution observed at $\theta_{12} \geq 80°$ in the polar plot.

Now we briefly discuss the mechanism of the recurrent hydrogen migration. Because of the high isomerization barrier from the acetylene to vinylidene (~2 eV), the hydrogen migration is expected to proceed in the picosecond time scale in the lowest triplet ($X^3\Sigma_g^-$) or singlet ($a^1\Delta_g$) electronic states [20], which explains the component remaining in the acetylene configuration at $\Delta t =$ 90 fs [see Fig. 4(b)]. The ultrafast migration to vinylidene should, therefore, be attributed to the contribution from electronically excited states, which can be populated by the interaction with the nonresonant intense (0.13 PW/cm^2) pump laser pulse. In the first excited triplet state, $1^3\Pi$ (located 5.3 eV above the $X^3\Sigma_g^-$ state), for example, the acetylene configuration is unstable [20], so that the isomerization can proceed directly to reach the vinylidene configuration in a short time scale.

The subsequent backward isomerization to acetylene can be interpreted as the result of the internal conversion from the excited states to the ground $X^3\Sigma_g^-$ state. Once the vinylidene isomer is formed in the ground state in such a manner, the isomerization to the more stable acetylene isomer in the ground state [17,19,20] should rapidly proceed because the vibrational energy is sufficiently high to overcome the isomerization barrier (~0.4 eV [20]). The longer time scale of the backward migration as well as the broad distribution after the recurrence would be attributed to the spread of the nuclear wave packet due to the intramolecular vibrational redistribution to other vibrational modes.

In conclusion, we demonstrated the real-time tracking of ultrafast hydrogen migration in the molecular frame with deuterated acetylene dication as the target. The time-resolved Coulomb explosion imaging employed here has wide applicability to unveil the intramolecular hydrogen dynamics, for instance, in neutral molecules, by using a tunable ultrashort laser pulse to resonantly trigger photochemical reactions of interest. The direct visulization of rapidly migrating hydrogen will provide a deeper understanding of chemical reactions of hydrocarbons as well as new prospects for efficient coherent reaction control with tailored laser pulses.

The authors thank Dr. J.-C. Delagnes for valuable discussion. The present work is supported by the Grant in Aid for Priority Areas for Control of Molecules in Intense Laser Fields from MEXT of Japan.

*hishi@ims.ac.jp

[1] H. F. Schaefer III, Acc. Chem. Res. **12**, 288 (1979).
[2] A. M. Mebel *et al.*, J. Am. Chem. Soc. **118**, 9759 (1996).
[3] Y. Wakatsuki *et al.*, J. Am. Chem. Soc. **113**, 9604 (1991).
[4] A. Hishikawa *et al.*, J. Electron Spectrosc. Relat. Phenom. **141**, 195 (2004).
[5] A. N. Markevitch *et al.*, Phys. Rev. Lett. **96**, 163002 (2006).
[6] K. M. Ervin *et al.*, J. Chem. Phys. **91**, 5974 (1989).
[7] T. Osipov *et al.*, Phys. Rev. Lett. **90**, 233002 (2003).
[8] J. H. Posthumus, Rep. Prog. Phys. **67**, 623 (2004).
[9] F. Légaré *et al.*, Phys. Rev. A **71**, 013415 (2005).
[10] Z. Vager, Adv. At. Mol. Opt. Phys. **45**, 203 (2001).
[11] T. Ergler *et al.*, Phys. Rev. Lett. **95**, 093001 (2005).
[12] E. Skovsen *et al.*, Phys. Rev. Lett. **89**, 133004 (2002).
[13] A. Hishikawa *et al.*, J. Chem. Phys. **122**, 151104 (2005).
[14] F. Légaré *et al.*, Phys. Rev. A **72**, 052717 (2005).
[15] M. P. Jacobson *et al.*, J. Phys. Chem. **104**, 3073 (2000).
[16] J. Levin *et al.*, Phys. Rev. Lett. **81**, 3347 (1998).
[17] D. Duflot *et al.*, J. Chem. Phys. **102**, 355 (1995).
[18] M. J. Jensen *et al.*, Phys. Rev. Lett. **84**, 1128 (2000).
[19] R. Thissen *et al.*, J. Chem. Phys. **99**, 6590 (1993).
[20] T. S. Zyubina *et al.*, J. Chem. Phys. **123**, 134320 (2005).
[21] H. Hasegawa *et al.*, Chem. Phys. Lett. **349**, 57 (2001).
[22] A. Hishikawa *et al.*, Phys. Rev. Lett. **97**, 243002 (2006).
[23] M. V. Ammosov *et al.*, Sov. Phys. JETP **64**, 1191 (1986).